SCHEDAE INFORMATICAE
VOLUME 20 (2011) DOI 10.4467/20838476SI.11.006.0292

Proximal Bundle Method for a Simplified Unilateral Adhesion Contact Problem of Elasticity

Jerzy Czepiel
Institute of Computer Science, Jagiellonian University,
Łojasiewicza 6, 30-348 Kraków, Poland
e-mail: *czepiel@ii.uj.edu.pl*

Abstract. We consider a mathematical model which describes the adhesive contact between a linearly elastic body and an obstacle. The process is static and frictionless. The normal contact is governed by two laws. The first one is a Signorini law, representing the fact that there is no penetration between a body and an obstacle. The second one is a Winkler type law signifying that if there is no contact, the bonding force is proportional to the displacement below a given bonding threshold and equal to zero above the bonding threshold. The model leads to a variational-hemivariational inequality. We present the numerical results for solving a simple two-dimensional model problem with the Proximal Bundle Method (PBM). We analyze the method sensitivity and convergence speed with respect to its parameters.

Keywords: linearly elastic body, Winkler law, unilateral contact, adhesion, variational-hemivariational inequality, proximal bundle method.

1. Introduction

The laws which describe contact between an elastic body and a foundation often are discontinuous, nonmonotone and multivalued. Such laws lead to problems which can be represented by means of hemivariational inequalities (HVIs) which have been introduced by Panagiotopoulos in 80's (see for example [17]). The requirement for the contact law to be possible to describe by means of HVI is the existence of a locally Lipschitz superpotential such that the multivalued law corresponds to its Clarke subdifferential. This is not possible for a nonpenetration Signorini law for which

the (convex) superpotential assumes infinite values. Therefore solving the contact problems which involve both nonmonontonicity and infinite values (which is the case in nonpenetration problems) requires the so called variational – hemivariational inequalities.

Hemivariational inequalities describing various problems of contact mechanics were investigated for example in [17] and, later, in [15]. Variational – hemivarional inequalities in the context of contact mechanics were studied, among others, by Panagiotopoulos [18], Motreanu [16], Liu [11, 12], Carl [2] and Kovtunenko [8, 10].

This article deals with the numerical solution of variational hemivariational inequalities. We consider a static problem which represents a simplified model of unilateral adhesive contact between a linear elastic body and a foundation. The adhesive law similar to the one used in this article (see formulae (8)–(9) in the sequel) was used in [7] (Example 6.4) and [6] (Application 6.6.8).

After discretization using the Finite Element Method (FEM), a variational-hemivariational inequality can be represented as the nonconvex optimization problem [7]. This problem can be solved numerically using the nonsmooth optimization methods like the Proximal Bundle Method or the Bundle Newton Method. Such approach is used in [7] (see also [13, 14]). The Proximal Bundle Method (PBM) has parameters which are to be chosen arbitrarily (Makela [13, 14] describes the method of the adaptive choice of one parameter u_k which is key for the convergence rate). The main aim of this article is to investigate the sensitivity of the PBM applied to a variational – hemivariational inequality describing the adhesive unilateral contact with respect to these parameters. The convergence rate for the PBM is known to be very slow: for the convex potential one requires $O(1/\epsilon^3)$ iterations to obtain the error of order ϵ (see [9]). Here we present the numerical convergence rate analysis for the nonconvex problem originating from the adhesive contact model.

The example problem used for computations is similar to the delamination problem used as a benchmark in [7] (Example 6.4), however, the structured finite element mesh used in this article consists of the rectangles with two diagonals (so called crossed mesh) and such mesh in known to avoid the numerical locking effects in elasticity problems in contrast to the mesh with one diagonal [1]. For the benchmark problem the detailed analysis of the PBM convergence with respect to the parameter choice is presented.

The structure of the article is the following. After Section 2 in which the required definitions are introduced, we present the abstract problem in Section 3. In Section 4 the PBM method is recalled. Section 5 presents the benchmark problem used for computations. Section 6 is divided into few parts presenting sensitivity tests and conclusions.

2. The notation and definitions

Let $\Omega \subset \mathbb{R}^d$, where $d \in \{2, 3\}$ be a nonempty, open and bounded set with a regular (Lipschitz) boundary. This set is occupied by the linearly elastic body. The bound-

ary of Ω is separated into three pairwise disjoint subsets $\partial\Omega = \bar{\Gamma}_C \cup \bar{\Gamma}_D \cup \bar{\Gamma}_N$. We denote the space of second order symetric tensors on $\mathbb{R}^d$ by $\mathbb{S}^d$. We use $\cdot$ and $|\cdot|$ as the scalar product and the euclidean norm on $\mathbb{R}^d$ and $\mathbb{S}^d$ respectively. Moreover we shall use the notation

$$H = L^2(\Omega)^d = \{\, u = (u_i) \,|\, u_i \in L^2(\Omega) \,\},$$
$$Q = \{\, \sigma = (\sigma_{ij}) \,|\, \sigma_{ij} = \sigma_{ji} \in Q \,\},$$
$$H_1 = \{\, u = (u_i) \,|\, \varepsilon(u) \in Q \,\},$$
$$Q_1 = \{\, \sigma \in Q \,|\, Div\sigma \in H \,\}.$$

Here $\varepsilon : H_1 \to Q$ and $\mathrm{Div} : Q_1 \to H$ are the *deformation* and *divergence* operators, respectively, defined by

$$\varepsilon(u) = (\varepsilon_{ij}(u)), \quad \varepsilon_{ij}(u) = \frac{1}{2}(u_{i,j} + u_{j,i}),$$
$$\mathrm{Div}\,\sigma = (\sigma_{ij,j}),$$

where i and j run between 1 and d, and the sumation convention over repeated indices is adopted. Index after comma denotes a partial derivative with respect to the corresponding component of the independent variable.
We denote the normal and tangential components of σ by σ_ν and σ_τ. If σ is smooth enough, then

$$\sigma_\nu = (\sigma n) \cdot n,\ \sigma_\tau = \sigma n - \sigma_\nu n.$$

Definition 1. *The Clarke generalized directional derivative (see [3]) of a locally Lipschitz function $h : X \to \mathbb{R}$ at the point $x \in X$ in the direction $v \in X$, where X is a reflexive Banach space, denoted by $h^0(x; v)$, is defined by*

$$h^0(x; v) = \limsup_{y \to x, \lambda \searrow 0} \frac{h(y + \lambda v) - h(y)}{\lambda}.$$

The Clarke subdifferential of h at x denoted by $\partial_{Cl} h(x)$ is a subset of X^* given by

$$\partial_{Cl} h(x) = \{\, \xi \in X^* : h^0(x; v) \geq \langle \xi, v \rangle_{X^* \times X} \text{ for all } v \in X \,\}.$$

The subdifferential of a convex functional will be denoted by ∂_{Conv}.

3. The problem formulation

In this section we present a contact problem of elasticity as well as its weak formulation and the corresponding Galerkin problem. The body is assumed to be linearly elastic and the process is assumed to be static. Furthermore we need the following assumptions on the data:

$H(\mathcal{E})$: the elasticity operator $\mathcal{E} : \Omega \times \mathbb{S}^d \to \mathbb{S}^d$ is a bounded symmetric positive definite fourth order tensor, i.e.,

$$\begin{cases} (a)\ \mathcal{E}_{ijkl} \in L^\infty(\Omega),\ 1 \le i,j,k,l \le d, \\ (b)\ \mathcal{E}\sigma \cdot \tau = \sigma \cdot \mathcal{E}\tau,\ \forall\, \sigma, \tau \in \mathbb{S}^d,\ \text{a.e. in } \Omega, \\ (c)\ \mathcal{E}\tau \cdot \tau \ge m|\tau|^2\ \ \forall\, \tau \in \mathbb{S}^d,\ \text{a.e. in } \Omega \text{ with } m > 0. \end{cases} \tag{1}$$

$H(f)$: the force and the traction densities satisfy

$$f_0 \in L^2(\Omega)^d, \quad f_2 \in L^2(\Gamma_2)^d, \tag{2}$$

$H(\nu)$: the threshold at which the bonds between the body and the foundation break is denoted by $M > 0$ and the force rate of the bonds is denoted by $a > 0$.

Problem $\mathcal{P}_M$. *Find a displacement field $u : \Omega \to \mathbb{R}^d$ and a stress field $\sigma : \Omega \to \mathbb{S}^d$ such that*

$$\sigma = \mathcal{E}(\varepsilon(u)) \quad in \quad \Omega, \tag{3}$$

$$\operatorname{Div} \sigma + f_0 = 0 \quad in \quad \Omega, \tag{4}$$

$$u = 0 \quad on \quad \Gamma_D, \tag{5}$$

$$\sigma\nu = f_2 \quad on \quad \Gamma_N, \tag{6}$$

$$u_\tau = 0 \quad on \quad \Gamma_C, \tag{7}$$

$$u_\nu \le 0 \quad on \quad \Gamma_C, \tag{8}$$

$$-\sigma_\nu \in \begin{cases} [0,\infty) & if \quad u_\nu = 0 \\ \{a u_\nu\} & if \quad u_\nu \in (-M, 0) \\ [0, -aM] & if \quad u_\nu = -M \\ \{0\} & if \quad u_\nu < -M \end{cases} \qquad on \quad \Gamma_C. \tag{9}$$

The condition (7) means that there is no tangential displacement on the contact boundary. It is easy to observe that in the real situation the elastic body could displace tangentially on the boundary under the influence of the external and mass load. We see that the condition (7) is a simplification, but in some cases, especially when displacements are small it could be a good approximation of the real situation.

The normal contact multivalued law (8) means that there is no penetration between the body and the foundation while the law (9) means that if there is contact (i.e., $u_\nu = 0$) then the reaction force assumes some nonnegative value, and if there is no contact the bonding force is proportional to the displacement below the bonding threshold and equal to zero above the bonding threshold.

In order to formulate the laws (8) and (9) in the inclusion form, we introduce

the following functions

$$j_1(s) = \begin{cases} \frac{aM^2}{2} & \text{if } s < -M \\ \frac{as^2}{2} & \text{if } s \in [-M, 0] \\ 0 & \text{if } s > 0. \end{cases} \tag{10}$$

$$j_2(s) = \begin{cases} 0 & \text{if } s \leq 0 \\ +\infty & \text{if } s > 0. \end{cases} \tag{11}$$

Observe that these laws cannot be writen by means of the Clarke subdifferential only (since the notion of the Clarke subdifferential requires the function to be locally Lipschitz and in the presented case j_2 assumes infinite values). The functional j_1 is locally Lipschitz and j_2 is convex. Moreover (8)–(9) is equivalent to say that

$$-\sigma_\nu \in \partial_{Cl} j_1(u_\nu) + \partial_{Conv} j_2(u_\nu)$$

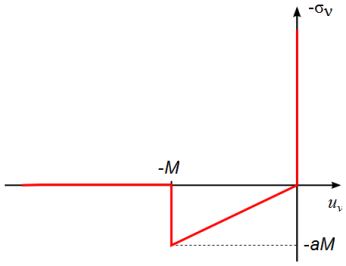

Fig. 1. The plot of the multivalued law used in the analyzed model

An important property of j_1 used in the sequel will be

$\underline{H(j_1)}$: for all $r \in \mathbb{R}$ and for all $\eta \in \partial_{Cl} j_1(u_\nu)$ we have $|\eta| \leq K$ with a positive real constant K.

3.1. The weak formulation and Galerkin method

We define the space

$$V = \{\, v \in H_1 : v = 0 \ \text{ on } \ \Gamma_D, v_\tau = 0 \text{ on } \Gamma_C \,\}.$$

Moreover we define an operator $A : V \to V^*$ by

$$\langle Au, v \rangle = \int_\Omega \mathcal{E}_{ijkl} \varepsilon_{ij}(u) \varepsilon_{kl}(v) \, dx$$

and a functional $f \in V^*$ by

$$\langle f, v\rangle = \int_\Omega f_0 \cdot v \; dx + \int_{\Gamma_N} f_2 \cdot v \; d\Gamma.$$

The norm in the space V is defined as $\|v\|_V^2 = \langle Av, v\rangle$. This expression defines the norm equivalent to the Sobolev norm $H^1(\Omega)^d$ due to the Korn inequality and $H(\mathcal{E})$. Furthermore we denote by $K \subset V$ the cone

$$K = \{v \in V : v_\nu \leq 0 \;\text{ on }\; \Gamma_C\}.$$

Now the weak formulation of our problem will be the following.

PROBLEM $\mathcal{P}_V$. *Find a displacement field $u \in K$ and $\xi \in L^2(\Gamma_C)$ such that $\xi \in \partial_{Cl} j_1(u_\nu)$ a.e. in Γ_C and for every $v \in K$ we have*

$$\langle Au - f, v - u\rangle + \int_{\Gamma_C} \xi(v_\nu - u_\nu)\, d\Gamma \geq 0. \tag{12}$$

The existence of solutions to the above problem is well known (see [6, 7]). For the sake of a numerical solution of the above problem we define the sequence of finite element spaces $\{V_n\}_{n=1}^\infty$ which are finite dimensional and approximate V from inside, i.e., $cl\,(\bigcup_{n=1}^\infty V_n) = V$. We denote $K_n = V_n \cap K$ and moreover we assume that $cl\,(\bigcup_{n=1}^\infty K_n) = K$. The Galerkin problem will be defined as follows.

PROBLEM $\mathcal{P}_{V_n}$. *Find a displacement field $u^n \in K_n$ and $\xi^n \in L^2(\Gamma_C)$ such that $\xi^n \in \partial_{Cl} j_1(u_\nu^n)$ a.e. in Γ_C and for every $v^n \in K_n$ we have*

$$\langle Au^n - f, v^n - u^n\rangle + \int_{\Gamma_C} \xi^n(v_\nu^n - u_\nu^n)\, d\Gamma \geq 0. \tag{13}$$

THEOREM 1. *Under assumptions $H(\mathcal{E}), H(f), H(\nu)$ if (u^n, ξ^n) is a sequence of solutions to $\mathcal{P}_{V_n}$, then for a subsequence we have $u^n \to u$ weakly in V and $\xi^n \to \xi$ weakly in $L^2(\Gamma_C)$ where u and ξ solve $\mathcal{P}_{V_n}$.*

For the proof of THEOREM 1 see [4].

3.2. The minimization problem

The numerical method will consist in solving the following minimization problem.

PROBLEM $\mathcal{M}_{V_n}$. *Find a displacement field $u^n \in K_n$ such that for the functional*

$$J_n(v) = \frac{1}{2}\langle Av, v\rangle - \langle f, v\rangle + \int_{\Gamma_C} j_1(v_\nu(x)) \; d\Gamma$$

we have $J_n(u^n) = \min_{v \in K_n} J_n(v)$.

THEOREM 2. *For every n the functional* J_n *has a global minimum over* K_n. *Moreover this minimum is a solution of* $\mathcal{P}_{V_n}$.

For the proof of THEOREM 2 see [4].

Let us assume that $\{v_1, \ldots, v_n\}$ is a base of V_n. We define $\Pi_n : V_n \to \mathbb{R}^n$ as the mapping which associates to the function $v \in V_n$ its coordinates in this base. Now $\mathbb{K}_n$ will be the cone defined as $\Pi_n(K_n)$. The problem $\mathcal{M}_{V_n}$ can be equivalently reformulated as follows.
Problem $\mathcal{M}_{\mathbb{R}^n}$**:** *Find* $x = (x_1, \ldots, x_n) \in \mathbb{K}_n$ *such that for the functional*

$$\mathbb{J}_n(z) = \frac{1}{2} z^T \mathbb{A} z - F^T z + \int_{\Gamma_C} j_1 \left(\left(\sum_{i=1}^{n} z_i v_i \right)_{\nu} (z) \right) \, d\Gamma$$

we have $\mathbb{J}_n(x) = \min_{z \in \mathbb{K}_n} \mathbb{J}_n(z)$.
In the above problem the matrix $\mathbb{A}$ is defined as $\mathbb{A} = \{\langle Av_i, v_j \rangle\}_{i,j=1}^n$ and the vector $\mathbb{F}$ as $\mathbb{F} = \{\langle f, v_i \rangle\}_{i=1}^n$.
Obviously u_n solves $\mathcal{M}_{V_n}$ if and only if $\Pi_n(u_n)$ solves $\mathcal{M}_{\mathbb{R}^n}$. Numerically we will solve this problem using the Proximal Bundle Method.

4. Proximal Bundle Method

The Proximal Bundle Method is used for nonsmooth and nonconvex optimization of locally Lipshitz functionals. It can be used as a blackbox tool to minimize a functional $\mathbb{J}_n : \mathbb{K}_n \to \mathbb{R}$ provided for any $x \in \mathbb{K}_n$ we can compute $\mathbb{J}_n(x)$ and we can find (one of possibly many) $\eta \in \partial_{Cl} \mathbb{J}_n(x)$.
The method is well known (see [13, 14]) and has been used in the context of hemivariational inequalities (see [7]) however it uses many parameters which are somewhat arbitrary in choice and no sensititvity analysis of the method with respect to the parameter choice in application to hemivariational inequalities is known. This article aims to fill this gap.
The main idea of the method is the construction of two sequences $x_i, y_i \in \mathbb{R}^n$. The points x_i will converge to the minimum of $\mathbb{J}_n$ and y_i will be the auxiliary points at which the subdifferentials will be computed and accumulated during the course of the algorithm. The elements of $\partial_{Cl} \mathbb{J}_n(y_i)$ which will be computed during the algorithm will be denoted by η_i. The starting point for the iteration can be arbitrary $x_1 = y_1$. In our case $x_1 = y_1 = 0$.

Each iteration step consists of two phases:

(1) Direction finding.

(2) Line search.

Direction finding. In the k-th iteration step we have two sequences of points x_j, y_j and a set of subgradients η_j, where $j \in \{1, \ldots, k\}$. The main aim of the direction finding phase is to find the direction $d_k \in \mathbb{R}^n$. The idea is to approximate the functional $\mathbb{J}_n$ by the piecewise linear function $\hat{\mathbb{J}}_n^k$ defined below.

$$\hat{\mathbb{J}}_n^k(x) = \max_{j \in \{1,\ldots,k\}} \{\mathbb{J}_n(y_j) + \eta_j^T(x - y_j)\},$$

which can be written as

$$\hat{\mathbb{J}}_n^k(x) = \max_{j \in \{1,\ldots,k\}} \{\mathbb{J}_n(x_k) + \eta_j^T(x - x_k) - \alpha_j^k\},$$

where α_j^k is the linearization error defined by

$$\alpha_j^k = \mathbb{J}_n(x_k) - \mathbb{J}_n(y_j) - \eta_j^T(x_k - y_j) \text{ for all } j \in \{1, \ldots, k\}.$$

If the functional $\mathbb{J}_n$ is convex, then it is easy to show that

$$\hat{\mathbb{J}}_n^k(x) \leq \mathbb{J}_n(x) \text{ for all } x \in \mathbb{R}^n$$

and $\alpha_j^k \geq 0$ for all $j \in \{1, \ldots, k\}$ (see [14]). In the nonconvex case $\hat{\mathbb{J}}_n^k(x)$ could be greater than $\mathbb{J}_n(x)$ and α_j^k could be less than zero. It is the reason why α_j^k was replaced by the subgradient locality measure (see [13]). It is

$$\beta_j^k = \max\{|\alpha_j^k|, \gamma(s_j^k)^2\},$$

where $\gamma \geq 0$ is the distance measure parameter and s_j^k defined by

$$s_j^k = \|x_j - y_j\| + \sum_{i=j}^{k-1} \|x_{i+1} - x_i\|$$

is the distance measure. Note that $\beta_j^k \geq 0$ for all $j \in \{1, \ldots, k\}$.
To calculate the search direction d_k we replace the original problem by the cutting plane problem (see [13],[14]).

PROBLEM CP

$$\begin{cases} \textit{minimize } \hat{\mathbb{J}}_n^k(x_k + d) + \frac{1}{2}u_k d^T d \\ \textit{subject to } x_k + d \in \mathbb{K}_n, \end{cases}$$

where $\frac{1}{2}u_k d^T d$ is the regularizing quadratic penalty term. This regularization is needed to guarantee the existence of the solution d_k. The parameter u_k is added to improve the convergence rate and to accumulate some additional information about the curvature of $\mathbb{J}_n$ around x_k (see [13, 14]).
The problem CP is still a nonsmooth optimization problem but it can be rewritten as a smooth quadratic programming problem.

PROBLEM QP *Find the solution* $(d_k, v_k) \in \mathbb{R}^{n+1}$ *of*

$$\begin{cases} \textit{minimize } v + \frac{1}{2}u_k d^T d \\ \textit{subject to } -\beta_j^k + \eta_j^T d \leq v \textit{ for all } j \in \{1, \ldots, k\} \textit{ and } x_k + d \in \mathbb{K}_n. \end{cases}$$

This problem is well known and can be solved by standard convex quadratic programming algorithms [13]. In the computations we used the library for quadratic programming, which is based on the method proposed in [5]. This method is based on the Sequential Minimal Optimization algorithm with an improved working set selection strategy.

Line search. In this phase we are looking for the most appropriate values for x_{k+1} and y_{k+1}. Notice that d_k calculated in the previous section minimizes only the approximation $\hat{\mathbb{J}}_n^k$ so $x_{k+1} = x_k + d_k$ is not necessarily the best possible value. We know that d_k is a good direction, now we consider the problem of determining how long should be the step size into that direction. We assume that $m_L \in (0, \frac{1}{2})$, $m_R \in (m_L, 1)$ and $\bar{t} \in (0, 1]$ are fixed method parameters. Firstly we search for the largest number $t_L^k \in [0, 1]$ such that $t_L^k \geq \bar{t}$ and

$$\mathbb{J}_n(x_k + t_L^k d_k) \leq \mathbb{J}_n(x_k) + m_L t_L^k v_k, \tag{14}$$

where v_k is the descent ratio and $v_k = \hat{J}_n^k(x_k + d_k) - \mathbb{J}_n(x_k) < 0$. If such a parameter t_L^k exists we take a long step

$$x_{k+1} = x_k + t_L^k d_k,\ y_{k+1} = x_{k+1}.$$

Otherwise, if (14) holds but $0 < t_L^k < \bar{t}$, then a short step

$$x_{k+1} = x_k + t_L^k d_k,\ y_{k+1} = x_k + t_R^k d_k$$

is taken, where $t_R^k > t_L^k$ and

$$-\beta_{k+1}^{k+1} + \eta_{k+1}^T d_k \geq m_R v_k. \tag{15}$$

If $t_L^k = 0$, then we take a null step

$$x_{k+1} = x_k,\ y_{k+1} = x_k + t_R^k d_k.$$

In the long step we have a significant decrease in the value of the functional $\mathbb{J}_n$ and there is no need for detecting discontinuities in the gradient of $\mathbb{J}_n$. In the short step and the null step there exists discontinuity in the gradient of $\mathbb{J}_n$. Then the formula (15) ensures that x_k and y_{k+1} lie on the opposite sides of this discontinuity, and a new subgradient will force an important modification on the next direction finding phase. In the computations a simple bisection algorithm is used for finding t_L^k and t_R^k. In both cases we take the biggest possible values.

Stop criterion. The iteration is terminated if $v_k \geq -\varepsilon_s$, where $\varepsilon_s > 0$ is a final accuracy tolerance supplied by the user (see [13, 14]).

The method has five parameters $(u_k, \gamma, \bar{t}, m_L, m_R)$. In the sequel we analyze the convergence speed with respect to these parameters.

5. The problem setup

The computations were performed on an academic two dimensional example. The physical setting is shown in Fig. 2.

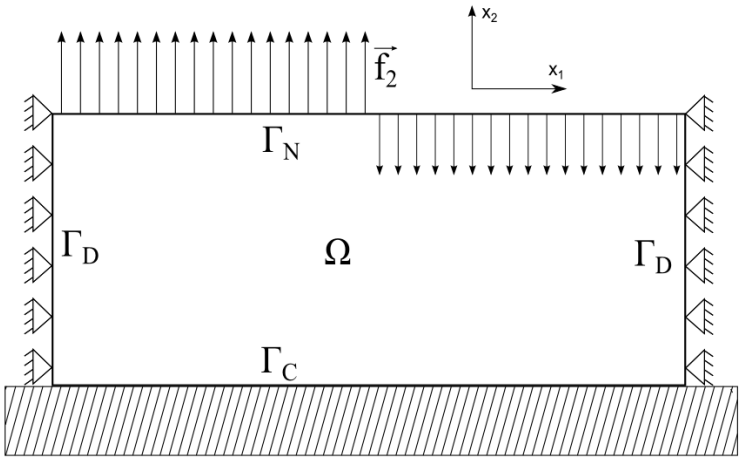

Fig. 2. The physical setup for the test problem

We assume that $\Omega = (0, L_1) \times (0, L_2) \subset \mathbb{R}^2$ and the boundary is divided into regions $\Gamma_D = \{0\} \times (0, L_2) \cup \{L_1\} \times (0, L_2)$, $\Gamma_N = (0, L_1) \times \{L_2\}$ and $\Gamma_C = (0, L_1) \times \{0\}$. The two dimensional example can be treated as an approximation for a three dimensional case if domain Ω is the cross-section of a three dimensional linear elastic body. In our case the body is assumed to be thin such that the plane stress hypothesis can be assumed. We furthermore assume that the body is isotropic and homogeneous so that the constitutive tensor can be described using only two parameters: the Young modulus E and the Poisson ratio ν. The exact form of the constitutive tensor used in the computations is the following

$$(\mathcal{E}\tau)_{\alpha\beta} = \frac{E\nu}{1-\nu^2}(\tau_{11} + \tau_{22})\delta_{\alpha\beta} + \frac{E}{1+\nu}\tau_{\alpha\beta}, \qquad 1 \leq \alpha, \beta \leq 2, \tag{16}$$

where $\delta_{\alpha\beta}$ is the Kronecker symbol.

The following data was used in the computations

$$L_1 = 40\,cm,\ L_2 = 4\,cm,\ \nu = 0.33,\ E = 69\,GPa.$$

The values ν, E correspond to the physical properties of aluminium. The forces were assumed to be the following

$$f_0 \equiv (0, 0), \quad f_2 = \begin{cases} (0, 0.69\,GPa) & \text{on } (0, L_1/2) \times \{L_2\}, \\ (0, -0.345\,GPa) & \text{on } (L_1/2, L_1) \times \{L_2\}. \end{cases}$$

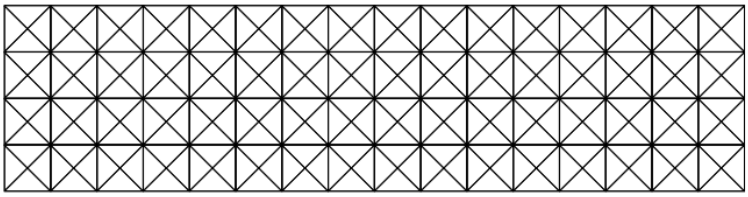

Fig. 3. The example mesh used in the computations for the test problem

The values used in the contact law chosen for the computations were

$$M = 2\ mm, a = 69\ GPa/m.$$

In order to avoid the numerical locking effects we used the structural crossed mesh of triangles as presented in Fig. 3.

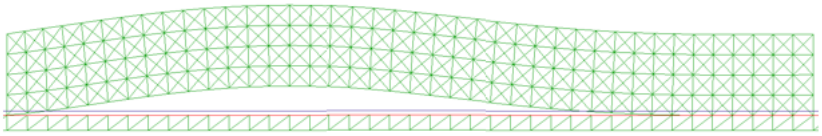

Fig. 4. The deformed mesh obtained as the computation result for the test problem

The deformed mesh after the computations for 710 degrees of freedom (mesh 40×4) is presented in Fig. 4. The normal stress and displacement on the contact boundary are presented in Fig. 5.

The verification of the method correctness is done via calculation of the residual and comparing it to the deformation obtained from the contact law. The computed total normal force and displacement values versus the ideal values from the contact boundary condition are presented in Fig. 6.

6. Tests of sensitivity

The convergence speed of the Proximal Bundle Method was tested for various values of its parameters. According to [13, 14] the key parameter is u_k. In the sequel we present the analysis of the convergence speed for various values of u_k and other parameters. The values of y_k in all the simulations were accumulated for 200 steps

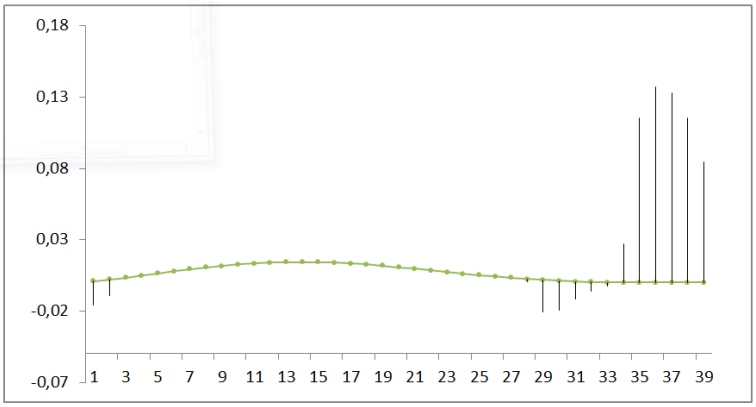

Fig. 5. The total normal force on every element and displacement on the contact boundary obtained for the test problem. The values are divided 4 times for visibility

of the iteration. After every 200 steps the stop criterion was checked and if it did not hold the points y_k were deleted from memory and the procedure was repeated starting from the obtained x_k.

6.1. Dependance of the convergence speed on u_k for the mesh 40×4

In this section the dependance of the convergence speed of the PBM on the choice of u_k for the mesh 40×4 (710 degrees of freedom) is analyzed. The minimal obtained values of the functional are summarized in Tab. 1. Moreover in this table the total number of iteration steps until the stop criterion was obtained as well as the number of long, short and null steps, respectively, are presented. The other parameters in this and the following simulations were: $\gamma = 0.5, m_L = 0.001, m_R = 0.5, \bar{t} = 0.003, \varepsilon_s = 10^{-13}$. The starting point for all the cases was the function constantly equal to 0.

Clearly for too small and too large u_k the convergence occurs after large number of steps comparing with the intermediate values of u_k. Moreover for large values of u_k we have mostly null steps, while for too small values we have mainly short steps. For the optimal u_k values (as it is clear from Tab. 1 these are values from 0.0007 to 0.001) we ave mostly short steps and some null steps. The fastest convergence rate equal to -14, i.e., $\mathbb{J}(x_k) - \mathbb{J}_{min} \approx Ck^{-14}$ was obtained for $u_k = 0.0008$. The rate close to -3 (in accordance with [9]) was obtained for $u_k = 0.0005$. For values $u_k = 5$ and $u_k = 0.5$ during the iteration history the discontinuity which was hard to pass was encountered and the objective did not improve significantly for many iterations as it is seen in the logartihmic graph.

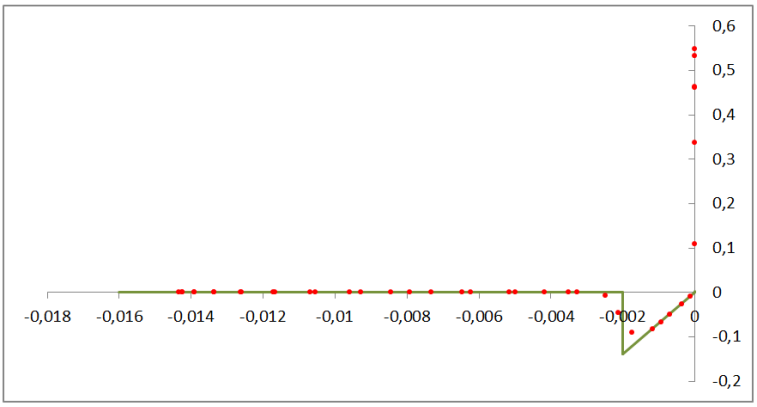

Fig. 6. The theoretical graph of the total normal force vs. the displacement on the contact boundary (continuous line) and the respective values obtained for the points on the boundary (dots)

6.2. Dependance of the convergence speed on u_k for the mesh 80×8

Now we present the analysis of the convergence speed of the PBM for the mesh 80×8 (2702 degrees of freedom). Since the Galerkin space V_n of admissible solutions is larger, the optimal objective value is smaller now. As it is clear from Tab. 2 and Fig. 8 the optimal u_k value is 0.0002 which corresponds to the value for the mesh 40×4 divided by 4. Moreover the optimal convergence rate is again about -14. We can hypothesise that $u_k \sim h^2$, where h is the mesh size parameter.

6.3. Dependance of the convergence speed on u_k for the mesh 160×16

The problem considered in this subsection has 10526 degrees of freedom. If the hypothesis that u_k should be proportional to h^2 is right, then the optimal value of u_k for this mesh should be about 0.00005. The numerical tests, as it is clear from Tab. 3 and Fig. 9 indeed show that for this value the convergence was fastest and the optimal objective value was only slighly worse than for $u_k = 0.00002$.

6.4. Tests of the PBM behavior for the changing u_k value

In [13] it is suggested that the adaptive changing of u_k should improve the algorithm efficiency. In order to test this, we took the solution obtained for the mesh 80×8 for $u_k = 0.0002$ using $\varepsilon_s = 10^{-13}$ and run the optimization algorithm again with

Tab. 1. Results of tests for various u_k values for the mesh 40×4

u_k	Iterations	$\mathbb{J}_{min}[10^{-4}]$	$\mathbb{J}(x_{1400})[10^{-4}]$	long	short	null
5	40200	–5,28865985	–5,27435748	4308	177	35715
0,5	6600	–5,28867025	–5,28839651	2573	179	3848
0,05	3000	–5,28867185	–5,28867134	1508	542	950
0,007	2200	–5,28867189	–5,28867187	98	1516	586
0,005	2000	–5,28867194	–5,28867193	39	1377	584
0,003	1800	–5,28867198	–5,28867198	0	1308	492
0,001	1600	–5,28867208	–5,28867208	0	1296	304
0,00095	1600	–5,28867207	–5,28867207	0	1323	277
0,0009	1400	–5,28867207	–5,28867207	3	1179	218
0,00085	1400	–5,28867208	–5,28867208	0	1255	145
0,0008	1400	–5,28867208	–5,28867208	0	1223	177
0,00075	1600	–5,28867206	–5,28867206	9	1343	248
0,0007	1600	–5,28867207	–5,28867207	5	1480	115
0,0005	31800	–5,28867157	–5,28855074	80	30804	916
0,00005	40200	–5,28866695	–5,28546276	82	40118	0

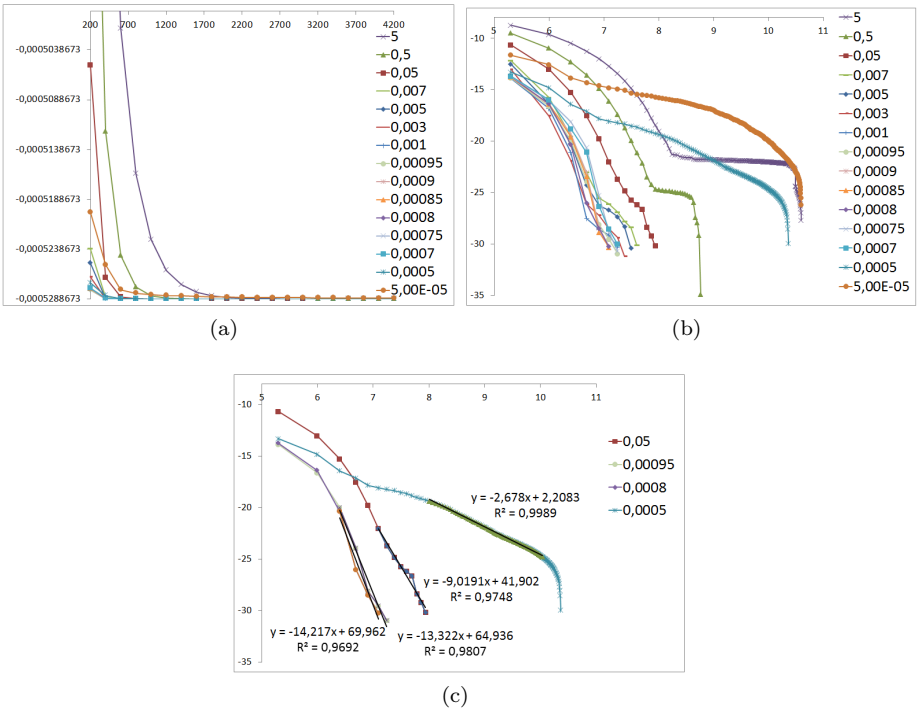

Fig. 7. The convergence history for various u_k values for the mesh 40×4. The graph (a) shows the iteration number (x axis) vs the objective value (y axis). The same graph with the logarithmic scale for both axes is depicted in the graph (b). Selected plots with fitted lines on the logarithmic scale are depicted in the graph (c)

Tab. 2. Results of tests for various u_k values for the mesh 80×8

u_k	Iterations	$\mathbb{J}_{min}[10^{-4}]$	$\mathbb{J}(x_{1400})[10^{-4}]$	long	short	null
0,005	5600	–5,37504353	–5,37396171	273	4794	533
0,0007	3400	–5,37504373	–5,37502537	0	3294	106
0,0005	2800	–5,37504377	–5,37503723	0	2656	144
0,00045	2800	–5,37504379	–5,37503989	0	2668	132
0,0004	2800	–5,37504381	–5,37504132	0	2716	84
0,00035	2600	–5,37504381	–5,37504232	0	2510	90
0,0003	2600	–5,37504382	–5,37504274	0	2494	106
0,00025	2600	–5,37504386	–5,37504347	0	2480	120
0,0002125	2400	–5,37504387	–5,37504370	0	2316	84
0,0002	2200	–5,37504380	–5,37504370	0	2091	109
0,00005	40200	–5,37504027	–5,37453342	1	40199	0
0,000005	40200	–5,37476454	–5,36815949	0	40200	0

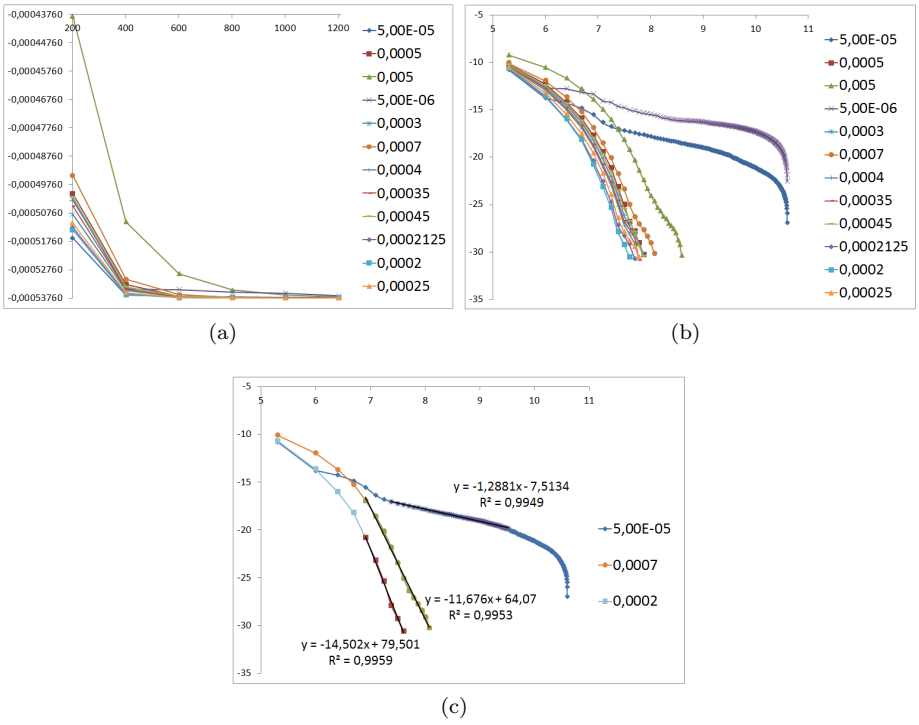

(a) (b)

(c)

Fig. 8. The convergence history for various u_k values for the mesh 80×8. The graph (a) shows the iteration number (x axis) vs the objective value (y axis). The same graph with the logarithmic scale for both axes is depicted in the graph (b). Selected plots with fitted lines on the logarithmic scale are depicted in the graph (c)

Tab. 3. Results of tests for various u_k values for the mesh 160×16

u_k	Iterations	$\mathbb{J}_{min}[10^{-4}]$	$\mathbb{J}(x_{1400})[10^{-4}]$	long	short	null
0,0001875	7200	–5,4006638	–5,3794895	0	7116	84
0,00008	6000	–5,4006639	–5,3920934	0	5953	47
0,00005	5600	–5,4006641	–5,3936754	0	5546	54
0,00002	7800	–5,4006642	–5,3942773	0	7608	192
0,000005	40200	–5,4001345	–5,3953643	0	40200	0

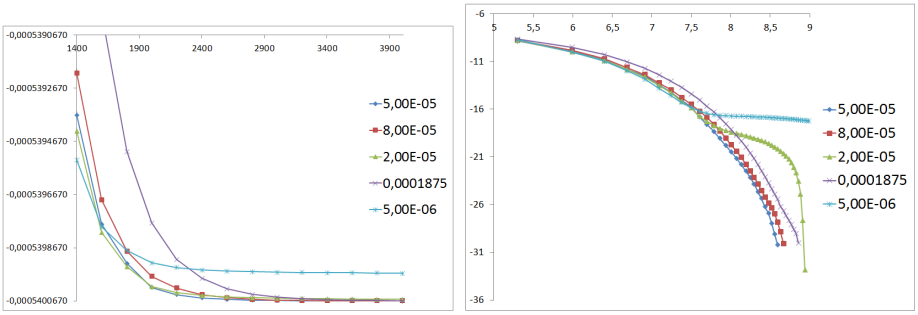

(a) (b)

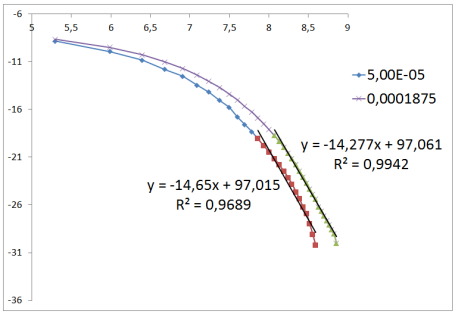

(c)

Fig. 9. The convergence history for various u_k values for the mesh 160×16. The graph (a) shows the iteration number (x axis) vs. the objective value (y axis). The same graph with the logarithmic scale for both axes is depicted in the graph (b). Selected plots with fitted lines on the logarithmic scale are depicted in the graph (c)

Tab. 4

u_k	Iterations	$\mathbb{J}_{min}[10^{-4}]$	long	short	null
200	1400	–5,375044024	32	29	1339
0,02	21400	–5,375044008	14	402	20984
0,002	800	–5,375043800	0	45	755
0,0002	3000	–5,375043802	0	930	2070
0,00002	2400	–5,375043806	0	613	1787
0,000002	600	–5,375043806	0	232	368

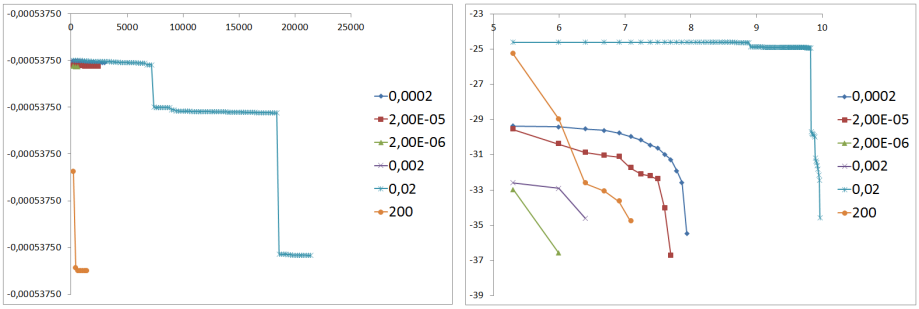

(a) (b)

Fig. 10. The plots showing the decrease of the objective value obtained after the iteration for the mesh 80×8 for the (best) value $u_k = 0.0002$. The solution was taken as the starting point for the iteration for various values of u_k. The plot (a) shows the objective value (y axis) vs. the number of iterations (x axis) and the same plot with logarithmic scales for both axes is shown in the plot (b)

$\varepsilon_s = 10^{-15}$ and various values of u_k taking the obtained solution as the starting point. The results, presented in Fig. 10 and Tab. 4, show, that the objective did not decrease significantly, so indeed the minimal value was found previously. The slight improvement of the minimal value was possible for the large values of u_k.

6.5. Dependence of the convergence speed on $\bar{t}$

Now we present the results of the tests of dependance of the convergence speed on the parameter $\bar{t}$. In this and the following sections the mesh 40×4 was considered and the value of u_k was assumed to be 0.00085. The results are depicted in Fig. 11 and Tab. 5. Clearly, the convergence speed and the optimal objective value is almost independent on the choice of $\bar{t}$. This parameter, however, influences the rate between the long and short steps. For small values of $\bar{t}$ almost all steps are long while for larger values we have almost only short steps.

Tab. 5. Results of tests for various $\bar{t}$ values for the mesh 40×4

$\bar{t}$	Iterations	$\mathbb{J}_{min}[10^{-4}]$	long	short	null
0,3	1400	–5,2886720846	0	1255	145
0,03	1400	–5,2886720846	0	1255	145
0,003	1400	–5,2886720846	0	1255	145
0,0003	1400	–5,2886720849	397	762	241
0,00003	1400	–5,2886720897	1055	175	170
0,0000003	1400	–5,2886720900	1159	14	227
3E-21	1400	–5,2886720900	1159	0	241

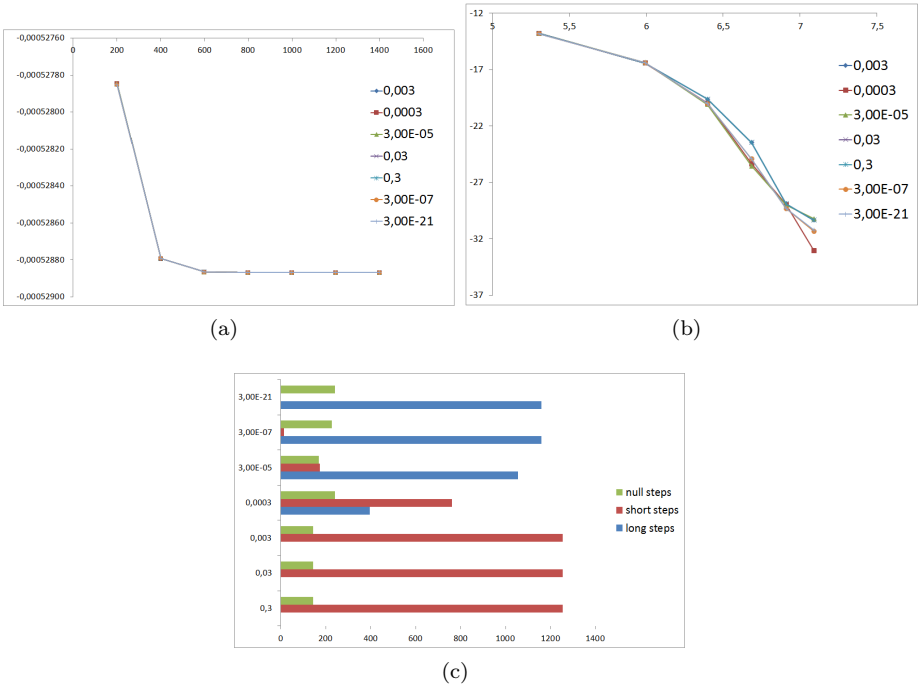

(a) (b)

(c)

Fig. 11. The behavior of the algorithm for the mesh 40×4 for various values of $\bar{t}$. The plot (a) presents the objective value vs. the number of the iteration steps. The same plots in the logarithmic scale are depicted in the plot (b). The plot (c) shows the relation between the number of the short and long steps

Tab. 6. Results of tests for various γ values for the mesh 40×4

γ	Iterations	$\mathbb{J}_{min}[10^{-4}]$	long	short	null
0,99999	1400	–5,288672113	0	1046	354
0,875	1200	–5,288672107	0	1012	188
0,8	1600	–5,288672103	1217	0	383
0,7	1600	–5,288672102	1265	0	335
0,6	1400	–5,288672076	1292	0	108
0,5	1400	–5,288672085	0	1255	145
0,25	20000	–5,288671623	195	18615	1190

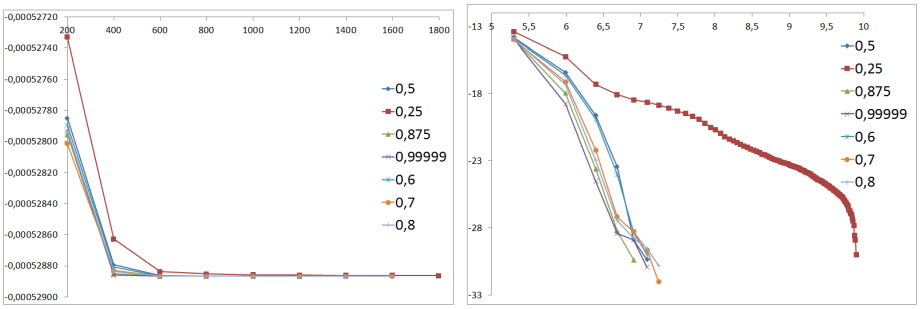

(a) (b)

Fig. 12. The behavior of the algorithm for the mesh 40×4 for various values of γ. The plot (a) presents the objective value vs. the number of the iteration steps. The same plots in the logarithmic scale are depicted in the plot (b)

6.6. Dependence of the convergence speed on γ

This section is devoted to the results of the tests of dependance of the convergence speed on the parameter γ. The results are depicted in Fig. 12 and Tab. 6. Clearly, for too small values of γ the algorithm behaves poorly. Above the certain threshold the convergence speed and the optimal objective value is almost independent on the choice of γ, with the best results obtained for values equal to about 0.9.

6.7. Dependence of the convergence speed on m_L and m_R

Now we present the results of the tests of dependance of the convergence speed on the parameters m_L and m_R. The results for m_L are depicted in Fig. 13 and Tab. 7 and the results for m_R are depicted in Fig. 14 and Tab. 8. Clearly, the convergence speed of the algorithm is not sensitive on the choice of these two parameters.

Tab. 7. Results of tests for various m_L values for the mesh 40×4

m_L	Iterations	$\mathbb{J}_{min}[10^{-4}]$	long	short	null
0,3	1600	–5,288672131	0	1195	405
0,2	1200	–5,288672127	0	1031	169
0,15	1600	–5,288672127	0	1320	280
0,1	1200	–5,288672122	0	998	202
0,05	1400	–5,288672103	0	1197	203
0,1	1200	–5,288672122	0	998	202
0,001	1400	–5,288672085	0	1255	145
0,0001	1400	–5,288672075	7	1210	183
0,000001	1600	–5,288672081	0	1384	216
1E-33	1600	–5,288672075	0	1328	272

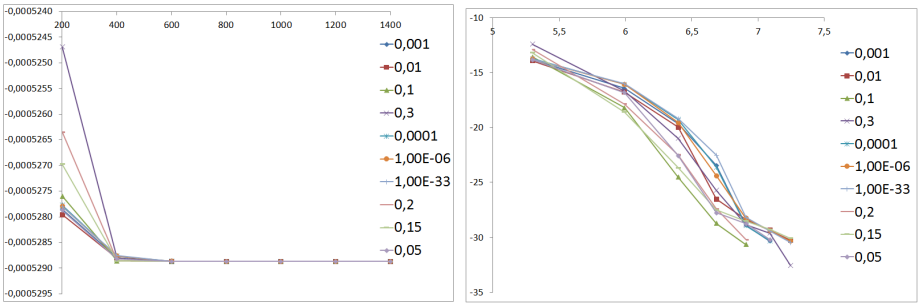

(a) (b)

Fig. 13. The behavior of the algorithm for the mesh 40×4 for various values of m_L. The plot (a) presents the objective value vs. the number of the iteration steps. The same plots in the logarithmic scale are depicted in the plot (b)

Tab. 8. Results of tests for various m_R values for the mesh 40×4

m_R	Iterations	$\mathbb{J}_{min}[10^{-4}]$	long	short	null
0,999	1400	–5,288672085	0	1255	145
0,7	1400	–5,288672085	0	1255	145
0,5	1400	–5,288672085	0	1255	145
0,1	1400	–5,288672085	0	1232	168
0,002	1600	–5,288672087	0	1282	318

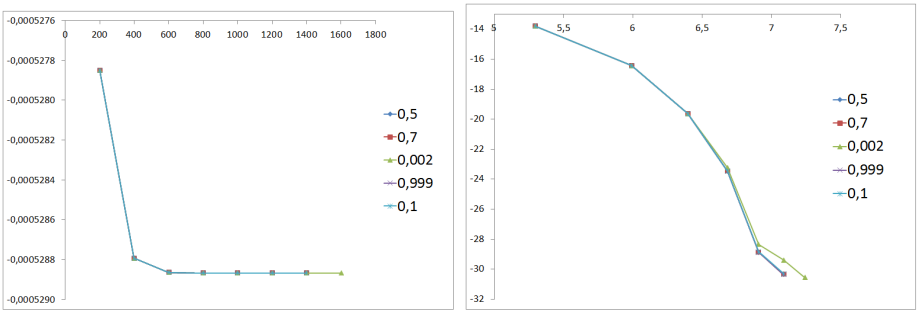

(a) (b)

Fig. 14. The behavior of the algorithm for the mesh 40×4 for various values of m_R. The plot (a) presents the objective value vs. the number of the iteration steps. The same plots in the logarithmic scale are depicted in the plot (b)

7. References

[1] Brezzi F., Fortin M.; *Mixed and hybrid finite element methods*, Springer-Verlag, New York 1991.

[2] Carl S.; *Existence and comparison results for variational-hemivariational inequalities*, Journal of Inequalities and Applications, 1, 2005, pp. 33–40.

[3] Clarke F.H.; *Optimization and Nonsmooth Analysis*, Wiley Interscience, New York 1983.

[4] Czepiel J., Kalita P.; *On numerical solution for a variational-hemivariational inequality modeling a simplified adhesion of linearly elastic body*, in preparation.

[5] Franc V., Hlavac V.; *A Novel Algorithm for Learning Support Vector Machines with Structured Output Spaces*, Research Report K333 22/06, CTU-CMP-2006-04, 2006. Available via `ftp://cmp.felk.cvut.cz/pub/cmp/articles/franc/Franc-TR-2006-04.ps`.

[6] Goeleven D., Motreanu D., Dumonte Y., Rochdi M.; *Variational and Hemivariational Inequalities: Theory, Methods and Applications*, Volume II: *Unilateral Problems*, Kluwer Academic Publishers, Dordrecht 2003.

[7] Haslinger J., Miettinen M., Panagiotopoulos P.D.; *Finite Element Method for Hemivariational Inequalities. Theory, Methods and Applications*, Kluwer Academic Publishers, Dordrecht 1999.

[8] Hintermüller M., Kovtunenko V., Kunisch K.; *Obstacle problems with cohesion: a hemivariational inequality approach and its efficient numerical solution*, SIAM Journal on Optimization, 21, 2011.

[9] Kiwiel K.C.; *Efficiency of proximal bundle methods*, Journal of Optimization Theory and Applications, 104, 2000, pp. 589–603.

[10] Kovtunenko V.; *A hemivariational inequality in crack problems*, Optimization, 1, 2010, pp. 1–19.

[11] Liu Z.; *On boundary variational–hemivariational inequalities of elliptic type*, Proceedings of the Royal Society of Edinburgh: Section A Mathematics, 140, 2010, pp. 419–434.

[12] Liu Z., Motreanu D.; *A class of variational–hemivariational inequalities of elliptic type*, Nonlinearity, 23, 2010, pp. 1741–1752.

[13] Mäkelä M.M.; *Nonsmooth Optimization, Theory and Applications with Applications to Optimal Control*, PhD Thesis, Jyväskylä 1990.

[14] Mäkelä M.M., Mietinen M., Lukšan L., Vlček J.; *Comparing Nonsmooth Nonconvex Bundle Methods in Solving Hemivariational Inequalities*, Journal of Global Optimization, 14, 1999, pp. 117–135.

[15] Migórski S., Ochal A.; *A unified approach to dynamic contact problems in viscoelasticity*, Journal of Elasticity, 83, 2006, pp. 247–276.

[16] Motreanu D., Winkert P.; *Variational-hemivariational inequalities with nonhomogeneous Neumann boundary condition*, Le Matematiche, 65, 2011, pp. 109–119.

[17] Naniewicz Z., Panagiotopoulos P.D.; *Mathematical theory of hemivariational inequalities and applications*, CRC, 1995.

[18] Panagiotopoulos P.D.; *Variational-hemivariational inequalities in nonlinear elasticity. The coercive case*, Applications of Mathematics, 33, 1988, pp. 249–268.

Received July 18, 2010